Evidence for local monoclinic structure, polarization rotation, and morphotropic phase transitions in $(1-x)BiFeO_3$-$xBaTiO_3$ solid solutions: A high-energy synchrotron x-ray powder diffraction study

Anar Singh,[1] Chikako Moriyoshi,[2] Yoshihiro Kuroiwa,[2] and Dhananjai Pandey[1,*]

[1]*School of Materials Science and Technology, Indian Institute of Technology (Banaras Hindu University), Varanasi -221005, India*

[2]*Department of Physical Science, Graduate School of Science, Hiroshima University, Higashi-Hiroshima, Hiroshima 739-8526, Japan*

(Received 22 May 2013; published 19 July 2013)

We have presented evidence for composition-driven rhombohedral-to-cubic and cubic-to-tetragonal morphotropic phase transitions in $(1-x)BiFeO_3$-$xBaTiO_3$ (BF-xBT) solid solutions at $x \approx 0.35$ and 0.85, respectively. It is shown that these transitions lead to the appearance of two peaks in the composition variation of dielectric constant, similar to that in well-known piezoelectric ceramics. The existing controversies about the true structure of the so-called cubic phase of BF-xBT are resolved using high-energy synchrotron x-ray powder diffraction data. It is shown that the ferroelectric cubic phase of BF-xBT has got locally monoclinic structure of M_A type in the Cm space group whose polarization vector rotates on its mirror plane on increasing the concentration of $BaTiO_3$ (x). The ferroelectric-to-paraelectric phase transition in pseudocubic monoclinic phase is shown to be of tricritical nature.

DOI: 10.1103/PhysRevB.88.024113 PACS number(s): 77.80.B−, 77.80.bg, 77.84.−s, 77.80.−e

I. INTRODUCTION

Magnetoelectric multiferroic materials are currently receiving much attention due to their potential for technological applications in several multifunctional sensor, actuator, data storage, and spinotronics devices.[1–3] Among the multiferroic materials, $BiFeO_3$ with a ferroelectric $T_C \sim 1103$ K (Ref. 4) and magnetic $T_N \sim 643$ K (Ref. 5) has attracted maximum attention as a promising room temperature multiferroic. It has got a rhombohedral structure in the $R3c$ space group and canted G-type antiferromagnetic (AFM) arrangement of the Fe^{3+} magentic moments with a superimposed spin cycloidal-type spatial incommensurate modulation of an approximate wavelength of ∼620 Å.[6] The net macroscopic magnetization on account of spin canting gets cancelled because of the cycloidal modulation of the spins. As a result, $BiFeO_3$ can exhibit only quadratic magnetoelectric coupling which is much weaker than the linear coupling.[7] In order to observe linear magnetoelectric coupling,[8] it is imperative to melt the spin cycloid. The spin cycloid of $BiFeO_3$ can be destroyed (1) by reducing the particle size to less than the periodicity of the cycloid spin structure,[9] (2) due to epitaxial strains in thin films,[10] (3) on application of high magnetic field (>18–20 Tesla),[11] and (4) by chemical substitutions at Bi and/or Fe sites.[12–16] Among these options, the melting of the spin cycloid can conveniently be achieved by forming solid solutions of $BiFeO_3$ with perovskite compounds like $BiMnO_3$, $LaFeO_3$, $CaTiO_3$, $BaTiO_3$, and $SrTiO_3$.[12–16] While $PbTiO_3$ substitution does not seem to lead to the melting of the spin cycloid,[17] $(Bi_{0.8}La_{0.2})(FeGa)$-$xPbTiO_3$ system does show weak ferromagnetism presumably due to the melting of the spin cycloid.[18]

Among the various solid solutions of $BiFeO_3$, the system $(1-x)BiFeO_3$-$xBaTiO_3$ (BF-xBT) has shown considerable potential as it exhibits significant net macroscopic magnetization[15,19,20] and ferroelectric polarization.[20–23] Further, linear magnetoelectric coupling has been confirmed at the atomic level in the BF-xBT system.[15,24] In addition, this solid solution system is a potential eco-friendly alternative to toxic piezoelectric ceramics containing lead (Pb), like $Pb(Zr_xTi_{1-x})O_3$ (PZT) and $(1-x)Pb(Mg_{1/3}Nb_{2/3})O_3$-$xPbTiO_3$ (PMN-xPT).[25] The BF-xBT system also shows superior high-temperature piezoelectric properties than PZT and PMN-xPT because of a much higher Curie temperature (∼760),[26,27] a significantly higher depolarization temperature T_d (∼750 K), and a stable piezoelectric coefficient d_{33} of 170 pC/N up to T_d[27] in marked contrast to commercial PZT ceramics whose typical T_C is ∼575 K and $T_d \sim 400$ K only, even though d_{33} is much higher for PZT ceramics.[25] Higher T_C's (∼775 K) have been reported in solid solutions of $PbTiO_3$ with $Bi(Me'Me'')O_3$, where the ratio of Me′ and Me″ cations maintains average +3 valence,[28–30] but the T_d of these systems is $\sim T_C/2$,[31] which is much lower than the T_d of BF-xBT, which makes the latter very attractive for high-temperature applications.

The origin of macroscopic magnetization due to spin canting after melting of the spin cycloid and magnetoelectric coupling in the BF-xBT system is well understood.[24] However, the origin of a peak in the d_{33} coefficient for a composition in the range 0.25 to 0.35, depending on the dopants[26,27,32] or sintering environment,[26] is not well understood. In Pb-based piezoelectric ceramics, it has been shown that the presence of bridging monoclinic phase(s) between tetragonal and pseudorhombohedral structures with flat energy surfaces is responsible for the high piezoelectric coefficients, as the polarization vector in the monoclinic phase(s) can rotate on a symmetry plane.[33] In the BF-xBT system also, the end members are rhombohedral ($BiFeO_3$: $R3c$ space group) and tetragonal ($BaTiO_3$: $P4mm$ space group). Are there bridging monoclinic phases between $R3c$ and $P4mm$ in this system as well? We seek to address this issue in this paper by examining the crystal structure of BF-xBT at room temperature as a function of composition using high-energy synchrotron x rays. We show that the intermediate phase of BF-xBT with apparent cubic structure is indeed locally monoclinic.

The crystal structure of BF-xBT solid solutions at room temperature has been quite controversial. In an early study, it was reported that the rhombohedral phase ($R3c$ space group) of $BiFeO_3$ persists up to 67% of $BiFeO_3$ (i.e. $x \leqslant 0.33$), while the tetragonal phase ($P4mm$ space group) of $BaTiO_3$ is stable for less than 7.5% of $BiFeO_3$ (i.e. $x > 0.925$).[34] For the compositions between $0.33 < x \leqslant 0.925$, the crystal structure was reported to be cubic in the $Pm\bar{3}m$ space group. While confirming these early observations on the room temperature crystal structures of the BF-xBT, Kumar *et al.*[35] also reported that the cubic compositions are paraelectric in nature.[35] However, this was questioned by Kim *et al.*[20] who along with many others[21–23] observed ferroelectric hysteresis loops (P-E loops) in the so-called cubic BF-xBT compositions also. Since the centrosymmetric cubic $Pm\bar{3}m$ space group cannot show ferroelectricity, Kim *et al.*[20] proposed noncentrosymmetric crystal structure in the $R3c$ space group for the cubic compositions for $x \leqslant 0.40$ and $R3c$ or $P4mm$ (unable to distinguish) space group for $0.40 < x \leqslant 0.6$ without any convincing diffraction evidence.[20] More recently, Kiyanagi *et al.*[36] have proposed that the structure of BF-xBT is purely rhombohedral (i.e. $BiFeO_3$ like) for $x < 0.20$, whereas for $x \geqslant 0.20$, a cubic phase starts appearing and coexists with the rhombohedral phase. Beyond $x = 0.60$, the cubic phase transforms into a tetragonal phase ($P4mm$, i.e. $BaTiO_3$ like) that coexists with the rhombohedral phase for $0.60 \leqslant x < 0.85$.[36] This implies that the ferroelectric hysteresis loops reported for the cubic compositions could be originating from the coexisting noncentrosymmetric $R3c$ and $P4mm$ phases. Evidently, there is no unanimity on the observation of ferroelectricity in the so-called cubic compositions. The existing controversies in the literature are mainly because there is no systematic structural study on chemically homogeneous samples of BF-xBT for the entire cubic composition range using the Rietveld refinement technique based on high-resolution and high-energy synchrotron x-ray powder diffraction data.

In this paper, we seek to resolve the existing controversies regarding the crystal structures of BF-xBT at room temperature by the Rietveld technique of structure refinement using rotating anode and high-resolution and high-energy synchrotron-based x-ray powder diffraction data for the composition range $0.05 \leqslant x \leqslant 1.0$ and $0.40 \leqslant x \leqslant 0.85$, respectively, with special emphasis on understanding the true structure of the so-called cubic phase. Our results reveal the existence of two morphotropic phase transitions in the BF-xBT system at $x \approx 0.35$ and $x \approx 0.85$. Further, we present evidence for the existence of local M_A-type monoclinic structure, in the average cubic structure of BF-xBT, which may act as a bridging phase, over a wide composition range ($0.35 \leqslant x \leqslant 0.85$). We also show using high-energy synchrotron x-ray powder diffraction (SXRPD) data that rotational instability (tilt) of oxygen octahedra of $BiFeO_3$ about the $\langle 111 \rangle$ pseudocubic (pc) axis persists at the local level even in the so-called cubic phase of BF-xBT for the $BiFeO_3$ rich compositions, and this instability decreases with decreasing $BiFeO_3$ concentration. By correlating the structural changes with the variation in the dielectric constant as a function of composition (x), we show that corresponding to the two morphotropic phase boundary (MPB) compositions, one observes peaks in the dielectric constant also. We also show that the polarization vector of the local monoclinic phase rotates by 10° away from the [001] tetragonal direction towards the [111] rhombohedral direction on increasing the $BiFeO_3$ content.

II. EXPERIMENTAL

BF-xBT powders were prepared by solid-state reaction route, the details of which are described elsewhere.[15,24,37,38] Laboratory x-ray powder diffraction (XRPD) measurements were carried out using an 18-kW rotating anode (CuK_α) based Rigaku powder diffractometer operating in the Bragg-Brentano geometry and fitted with a curved crystal monochromator in the diffraction beam. The data were collected in the 2θ range of 20° to 120° at a step of 0.02° for $0.05 \leqslant x \leqslant 1.0$. High-energy synchrotron x-ray powder diffraction experiments were performed using a large Debye-Scherrer camera equipped with an imaging plate as a two-dimensional detector installed at BL02B2 beam line in SPring-8[39] at a wavelength of 0.4110 Å for $0.40 \leqslant x \leqslant 85$.

Room temperature dielectric and impedance measurements were carried out using a Novocontrol Alpha-A High Performance Frequency Analyzer. For the dielectric measurements, BF-xBT pellets were gently polished with 0.25 μm diamond paste for about 5 min and then washed with acetone to clean the surface. Isopropyl alcohol was then applied to the polished surface for removing the moisture, if any, on the pellet surfaces. Fired-on silver paste was subsequently applied on both the faces of the pellets. It was first dried at 400 K in an oven and then cured by firing at 825 K for about 10 min.

III. RIETVELD REFINEMENT DETAILS

Rietveld refinements were carried out using the FULLPROF package.[40] The Wyckoff positions and the asymmetric unit for the various space groups used during the Rietveld refinements of phases of BF-xBT system in this paper are given below:

(i) For the rhombohedral phase with the $R3c$ space group, we used hexagonal axes with lattice parameters $a_H \approx b_H \approx \sqrt{2}\, a_{pc}$ and $c_H \approx 2\sqrt{3}\, a_{pc}$, where a_{pc} corresponds to the primitive pc cell parameter. There are three ions (Bi^{3+}/Ba^{2+}, Fe^{3+}/Ti^{4+}, and O^{2-}) in the asymmetric unit of the rhombohedral structure. Of them, Bi^{3+}/Ba^{2+} and Ti^{4+}/Fe^{3+} ions occupy the 6(a) Wyckoff site at (0, 0, z) while O^{2-} ions at the 18(b) sites at (x, y, z). Coordinates of all the atoms in the asymmetric unit cell of the $R3c$ space group can also be written as a function of the displacement parameters s, t, d, and e, as per Megaw *et al.* [41]: Bi^{3+}/Ba^{2+} (0,0,1/4 + s), Fe^{3+}/Ti^{4+} (0,0,t), O^{2-} (1/6 − 2e − 2d,1/3 − 4d,1/12).[41] The parameters s and t describe the polar displacement of cations Bi^{3+}/Ba^{2+} and Fe^{3+}/Ti^{4+} along $[111]_{rh}$ or $[001]_h$. The displacement parameter e of oxygen O^{2-} from its ideal position is related to the tilt angle (ω) of antiphase rotation of the oxygen octahedra about the trigonal $[111]_{rh}$ direction through the expression $\omega = \tan^{-1}(4e3^{1/2})$.[41] The parameter d is related to the distortion of the BO_6 (B: Fe^{3+}/Ti^{4+}) octahedra. The z coordinate of the oxygen ion is fixed at $z = 1/12$.[41]

(ii) For the cubic phase in the $Pm\bar{3}m$ space group, there are three ions (Bi^{3+}/Ba^{2+}, Fe^{3+}/Ti^{4+}, O^2) in the asymmetric unit with Bi^{3+}/Ba^{2+} ions occupying the 1(a) site at (0, 0, 0),

Ti^{4+}/Fe^{3+} the 1(b) site at (1/2, 1/2, 1/2), and O^{2-} at the 3(c) sites at (1/2, 1/2, 0). In the presence of local disorder in the structure, the cations and anions may occupy other Wyckoff sites as well.

(iii) For the tetragonal phase in the space group $P4mm$, there are four ions (Bi^{3+}/Ba^{2+}, Fe^{3+}/Ti^{4+}, O_I^{2-}, and O_{II}^{2-}) in the asymmetric unit with Bi^{3+}/Ba^{2+} ions occupying the 1(a) site at $(0, 0, z)$, Ti^{4+}/Fe^{3+} and O_I^{2-} the 1(b) site at $(1/2, 1/2, z)$, and O_{II}^{2-} the 2(c) site at $(1/2, 0, z)$. For refinements, Bi^{3+}/Ba^{2+} were fixed at the origin (0, 0, 0).

IV. RESULTS AND DISCUSSION

A. Structural evidence for two morphotropic phase transitions: Qualitative observations

Structural phase transitions occurring as a function of composition at a fixed temperature are called morphotropic phase transitions. For studying the room temperature crystal structure of BF-xBT as a function of composition (x), we first present a qualitative interpretation of the x-ray powder diffraction data. Figure 1 shows the XRPD profiles of the 222_{pc}, 400_{pc}, and 440_{pc} [all indices are with respect to a pc doubled perovskite cell] reflections after stripping off the CuKα_2 contribution for the rotating anode data on BF-xBT compositions in the range $0.10 \leqslant x \leqslant 1.0$. It is evident from this figure that, for compositions with $x < 0.34$, the 400_{pc} is a singlet, while 222_{pc} and 440_{pc} are doublets with weaker reflections occurring on the lower 2θ side, as expected for the rhombohedral structure of $BiFeO_3$. It is also evident from the figure that the peak splitting of 222_{pc} and 440_{pc} reflections decreases with increasing x. This suggests that the rhombohedral distortion of $BiFeO_3$ gradually decreases with $BaTiO_3$ substitution. For $x = 0.32$ and 0.34, the splitting of the 222_{pc} and 440_{pc} profiles is not clear, but asymmetric broadening on the left side of the 222_{pc} peak clearly reveals the presence of two overlapping peaks (marked with arrows in Fig. 1). Figure 2(a) depicts the evolution of the integrated intensity of the strongest superlattice reflection 311_{pc}, resulting from antiphase rotation of oxygen octahedra about the [111] rhombohedral axis, as a function of x. The integrated intensity of the 311_{pc} decreases linearly as a function of x and becomes zero at $x_c \approx 0.35$ as can be seen from Fig. 2(b). All these features confirm that the rhombohedral structure with $R3c$ space group is the stable phase of BF-xBT for $x < 0.35$.

For $0.36 \leqslant x \leqslant 85$, all the peaks in Fig. 1 appear to be singlets. This is the characteristic of a cubiclike phase with $Pm\bar{3}m$ space group. However, for $x \geqslant 0.90$, the XRPD profiles are markedly different from those corresponding to rhombohedral ($x \leqslant 0.34$) and the cubiclike ($0.36 \leqslant x \leqslant 85$) compositions. For example, an asymmetry on the lower 2θ side of the 400_{pc} reflection appears for $x \geqslant 0.90$, which suggests that the 400_{pc} is not a singlet. In order to get a clearer picture about the splitting of 400_{pc} peak, profile deconvolution was attempted, and the results are shown in Fig. 3. It is evident from this figure that the 400_{pc} peak consists of two reflections for $x = 0.96$, 0.94, and 0.90, while it is a singlet for $x = 0.85$. Similarly, the doublet nature of 440_{pc} peak is also revealed by the asymmetric broadening (marked with arrows in Fig. 1) of the 440_{pc} peak profile on the higher 2θ angle side. More significantly, the 222_{pc} is a singlet for $x \geqslant 0.90$. All these features correspond to the tetragonal structure with $P4mm$ space group. Thus, there are two composition-induced morphotropic phase transitions occurring at $x \approx 0.35$ and 0.85.

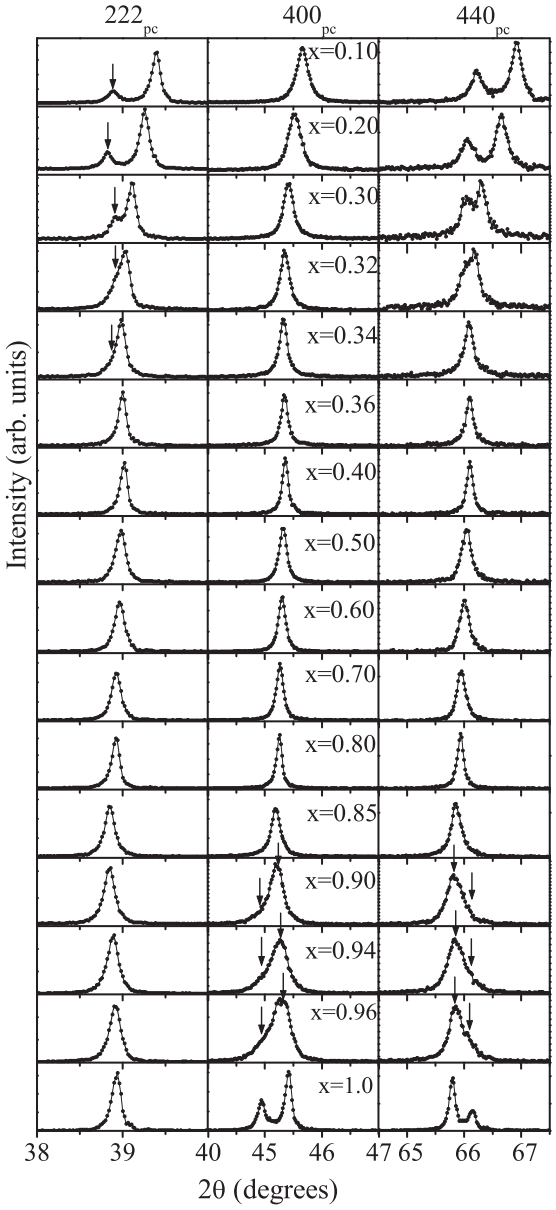

FIG. 1. Evolution of 222_{pc}, 400_{pc}, and 440_{pc} pc XRPD profiles for various compositions of BF-xBT with $x = 0.10$, 0.20, 30, 0.32, 0.34, 0.36, 0.40, 0.50, 0.60, 0.70, 0.80, 0.85, 0.90, 0.94, 0.96, and 1.0 at room temperature. Arrows indicate the doublet nature of the peaks.

B. Structural evidence for two morphotropic phase transitions: Rietveld refinement results

In order to confirm the qualitative observations of the previous section quantitatively, we carried out Rietveld analysis of XRPD data using the FULLPROF package. Figure 4 depicts the observed, calculated, and difference profiles obtained after the Rietveld analysis of the full XRPD patterns for four selected compositions with $x = 0.20$, 0.40, 0.80, and 0.94 using $R3c$,

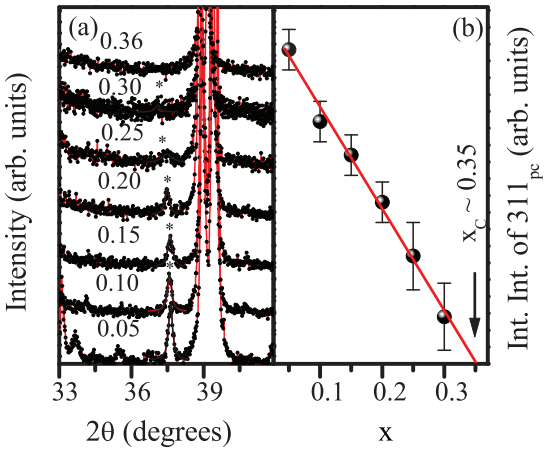

FIG. 2. (Color online) Evolution of the XRPD profile of (a) the strongest superlattice reflection 311_{pc} and (b) its integrated intensity for various compositions of BF-xBT with $x = 0.05$, 0.10, 0.15, 0.20, 0.25, 0.30, and 0.36 at room temperature.

$Pm\bar{3}m$, $Pm\bar{3}m$, and $P4mm$ space groups, respectively. The overall fit between the observed and calculated profiles is very good, with nearly flat difference profiles for all the four compositions. The results of the Rietveld refinement for selected compositions of BF-xBT are given in Table S1 in the Supplemental Material.[42] In order to compare the variation of unit cell parameters with compositions (x) of the three phases, we have calculated equivalent elementary perovskite cell parameters from the refined hexagonal c and a parameters using the following relationships:[41] $a \approx a_H/\sqrt{2}$ and $c \approx c_H/2\sqrt{3}$ for the rhombohedral phase. The variation in the elementary perovskite cell parameters for the composition range $0.0 \leqslant x \leqslant 1.0$, obtained from the Rietveld refinements, are shown in Fig. 5(a). It clearly reveals structural phase

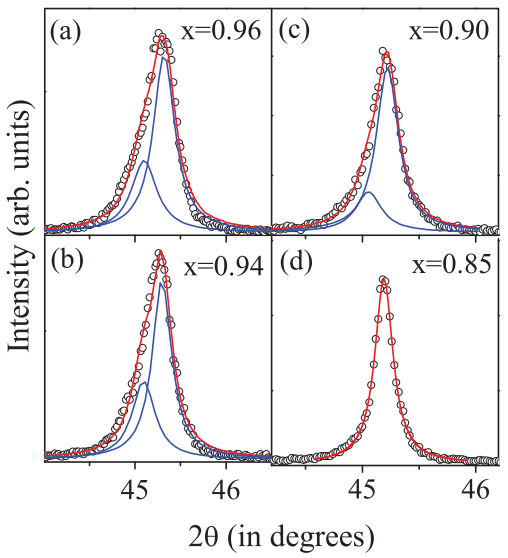

FIG. 3. (Color online) Observed (open circles) and deconvoluted (solid line) XRPD profiles of the 400_{pc} pc reflection of BF-xBT for (a) $x = 0.96$, (b) 0.94, and (c) 0.90. (d) For $x = 0.85$, the profile is symmetric due to its singlet nature.

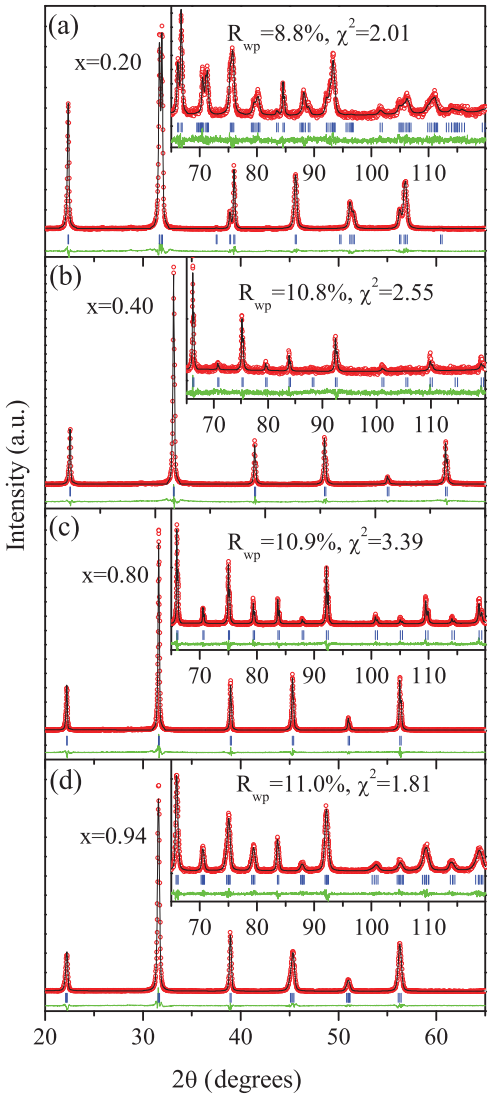

FIG. 4. (Color online) Observed (open circles), calculated (solid line), and difference (bottom line) patterns obtained from the Rietveld analysis of the room temperature x-ray powder diffraction data of BF-xBT for $x = 0.20, 0.40, 0.80$, and 0.94 using $R3c$, $Pm\bar{3}m$, $Pm\bar{3}m$, and $P4mm$ space groups, respectively. The vertical tick marks above the difference pattern stand for the Bragg peak positions. The insets in (a)–(d) depict the fits for high-angle reflections on a magnified scale.

transitions occurring around $x_c = 0.35$ from rhombohedral symmetry ($R3c$ space group) to cubiclike symmetry ($Pm\bar{3}m$ space group) and around $x = 0.85$ from cubiclike symmetry to the tetragonal symmetry ($P4mm$). The c/a ratio for the elementary perovskite cell shown in Fig. 5(b) shows that it systematically decreases with increasing x until it becomes 1.0 for $0.35 \leqslant x \leqslant 0.85$. The variation of the c/a ratio starts increasing again as a function of composition for $x > 0.85$. The variation of the c/a ratio as a function of x also reveals two structural phase transitions in BF-xBT occurring around $x_c = 0.35$ and $x = 0.85$. The unit cell volume depicted in Fig. 5(c) shows a significant change of slope across the two structural phase boundaries around $x_c = 0.35$ and $x = 0.85$. The refined equivalent isotropic thermal parameters (i.e., B_{iso} or B_{eq}; the anisotropic thermal parameters are given in the

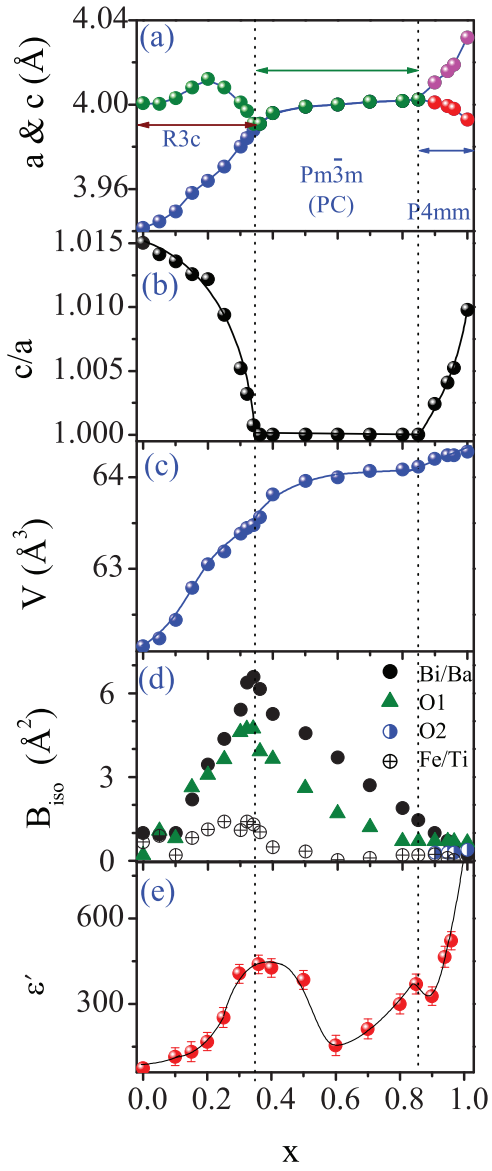

FIG. 5. (Color online) Variation in (a) unit cell parameters, (b) pseudotetragonality (c/a), (c) unit cell volume, (d) thermal parameters, and (e) dielectric constant (ε') of BF-xBT as a function of composition (x) in the composition range $0 \leqslant x \leqslant 1.0$ at room temperature.

Supplemental Material, Table S1 [Ref. 42) of A-, B-, and O-site ions are plotted as a function of x in Fig. 5(d). It is evident from this figure that the thermal parameters of the A and O sites increase anomalously with increasing concentration of $BaTiO_3$ in the rhombohedral phase and peak at the phase boundary between the $R3c$ and $Pm\bar{3}m$ structures at $x_c \approx 0.35$ with extremely large values. For compositions with $x > 0.35$, i.e. in the cubiclike region, the thermal parameters for both the sites (A and O) decrease with increasing x and drop to acceptable values in the tetragonal phase region. Interestingly, the thermal parameters for the B-site atoms are comparatively much smaller throughout the composition range $0.0 \leqslant x \leqslant 1.0$, as can be seen from Fig. 5(d).

C. Evidence for two morphotropic phase transition: Dielectric studies

The tetragonal-to-monoclinic morphotropic phase transition in PZT ceramics leads to peaking of the dielectric constant and piezoelectric properties at the MPB composition $x_c \sim 0.520$ and forms the basis of numerous technological applications of the PZT ceramics as electrochemical sensors and actuators.[43] Since BF-xBT shows two composition-induced phase transitions at $x_c \approx 0.35$ and 0.85, it is anticipated that, like in PZT, the dielectric constant of BF-xBT should show peaks at these two compositions.

The dielectric constant of BF-xBT samples shows very strong frequency dependence on account of the electrically heterogeneous microstructure with widely different resistivity of the grain boundaries and the grains in the sintered polycrystalline ceramics.[15] Since our BF-xBT samples were sintered in closed crucibles to prevent Bi^{3+} losses, the oxygen partial pressure inside the crucibles becomes low, as a result of which there is loss of oxygen during sintering. This loss can be written in the Kröger-Vink notation as follows:

$$O_0 \Leftrightarrow 1/2O_2V_0^{\cdot\cdot} + 2e'. \quad (1)$$

Electrons released due to oxygen vacancy V_0 may be captured by Fe^{3+} of BF-xBT, leading to its reduction to Fe^{2+}.

$$Fe^{3+} + 1e' \Leftrightarrow Fe^{2+}. \quad (2)$$

The presence of Fe^{2+} and Fe^{3+} ions leads to hopping of electrons, which increases the conductivity. During the cooling down period after sintering, the reverse process of reaction (1) occurs since the equilibrium concentration of vacancies decreases, but due to the insufficient time available during cooling and also the falling furnace temperature, the reoxidation process is restricted to the grain boundaries only.[15] Because of this, the grain boundaries regain their insulating properties, but the grains remain semiconducting due to the presence of Fe^{2+} and Fe^{3+} ions, giving rise to electrically heterogeneous microstructure. The hopping charge carriers in the grains would be stopped by the insulating grain boundaries, leading to enormously large space charge contributions to the measured dielectric constant. To understand the intrinsic dielectric response of BF-xBT as a function of composition, it is important to remove the contributions from the space charge effects. While the oxygen vacancies lead to space charge effects, they may not alter the structural features of BF-xBT solid solutions because of their extremely low concentrations close to the equilibrium concentration at the sintering temperatures.

Figures 6(a) and 6(b) show the variation in the dielectric constant (ε') and tanδ of BF-xBT, respectively, at room temperature for a few representative compositions with $x =$ 0.20, 0.40, 0.60, and 0.96 with frequency in the range 100 Hz to 1 MHz. It is evident from this figure that the value of dielectric permittivity is very high at lower frequencies but decreases with increasing frequency before stabilizing for $f > 200$ kHz, suggesting large space charge contributions at lower frequencies discussed in the previous paragraph. To determine the intrinsic dielectric constant of BF-xBT free from space charge contributions, one normally uses complex impedance (Z' and Z'') plots in the argand plane, the so-called

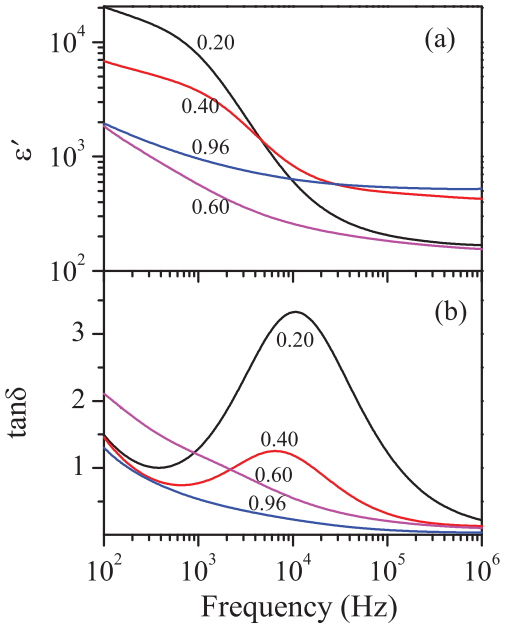

FIG. 6. (Color online) Variation of (a) the real part of dielectric constant (ε') and (b) tanδ of BF-xBT as a function of frequency for x = 0.20, 0.40, 0.60, and 0.96 at room temperature.

Cole-Cole plot.[44] Such plots for the above four compositions are shown in Fig. 7. It can be seen from Fig. 7(a) that there are two clear semicircular arcs with nearly no overlap for $x = 0.20$. Both the semicircular arcs are suppressed with their centers below the Z' axis. This suggests that dielectric relaxations associated with both the grains and the grain boundaries are polydispersive and deviate from the

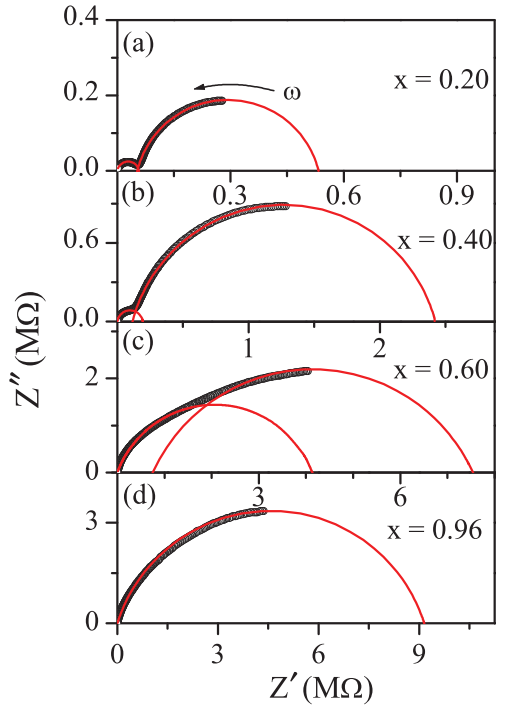

FIG. 7. (Color online) Cole-Cole impedance plot of BF-xBT for (a) $x = 0.20$, (b) 0.40, (c) 0.60, and (d) 0.96 at room temperature.

Debye relaxation model.[44] The low-frequency semicircular arc represents the contributions from the grain boundaries, while the high-frequency arc is due to the grains. With increasing x, the two arcs start overlapping with each other, as shown in Fig. 7(b) for $x = 0.40$, and finally tend to merge into each other at higher x, as can be seen from Fig. 7(c) for $x = 0.60$. As a result, for $x = 0.96$, only one semicircular arc is observed [see Fig. 7(d)], which means only bulk contribution is present at all the frequencies for such compositions. This gradual crossover from two to single circular arcs in the Cole-Cole plots is essentially due to decreasing Fe^{2+}/Fe^{3+} content, and hence hopping conductivity pathways with increasing x. It is interesting to note that the radius of the semicircular arc corresponding to grain contributions increases with increasing x. This reveals that the contribution from grain boundaries is more at the $BiFeO_3$-rich end, and it decreases with decreasing concentration of $BiFeO_3$. This effect can be clearly seen in Figs. 6(a) and 6(b), where the value of the dielectric constant of BF-xBT at low frequencies (grain boundary contributions) falls drastically with decreasing $BiFeO_3$ concentration. This is because, at high concentration of Fe, the effect of grain boundaries contribution is more, and it decreases with decreasing Fe concentration. The overlap between the two arcs suggests that the contributions from the grains cannot be separated from the grain boundaries for the intermediate frequency range in all the BF-xBT compositions. However, the value of dielectric constant at very high frequencies (say, 1 MHz) is nearly unaffected by the electrically heterogeneous microstructure for the entire composition range and represents the intrinsic contributions from the grains only.

Figure 5(e) shows the variation in the real part of the dielectric permittivity (ε') as a function of x for BF-xBT ceramics in the composition range $0.10 \leqslant x \leqslant 0.96$ for a measuring frequency of 1 MHz. The sample-to-sample variation of dielectric permittivity for each composition is shown by vertical error bars in the plot. It is well known in the literature that the room temperature dielectric permittivity of $BiFeO_3$ ($\sim$74 for single crystal)[45] is much lower than the dielectric permittivity of $BaTiO_3$ ($\sim$1000).[46] It is therefore expected that the dielectric permittivity of BF-xBT solid solutions would increase with increasing concentration of $BaTiO_3$. However, the variation of ε' with x shown in Fig. 5(e) is rather nonmonotonic with two peaks at $x = 0.35$ and 0.85. By analogy with the morphotropic phase transition in PZT where the peaking of ε' in ε'-x plot has been linked to a MPB (Ref. 25) effect involving tetragonal-to-monoclinic morphotropic phase transition,[25] the peaks in the ε'-x plot on BF-xBT also correspond to morphotropic phase transitions. However, unlike PZT, where one observes only one peak, we find evidence for two peaks in the BF-xBT system due to the presence of three different structural phase regions separated by two morphotroic phase boundaries around $x = 0.35$ and 0.85. Interestingly, peaking of the dielectric constant due to two morphotropic phase boundaries has been reported in the strongly piezoelectric ceramic material PMN-xPT (Ref. 47) also analogous to the two peaks in BF-xBT, but the two peaks occur at nearby compositions in PMN-xPT as compared to those in BF-xBT. In principle, PZT also possesses two phase boundaries as its structure changes from tetragonal ($P4mm$) to a pseudotetragonal monoclinic phase of M_A type (Cm) at

$x = 0.520$ and then from the pseudotetragonal monoclinic phase to the pseudorhombohedral monoclinic phase, also of M_A type in the Cm space group, at $x \approx 0.530$. However, the second phase at $x = 0.530$ does not involve a change of space group which remains Cm, and only the c_{pc}/a_{pc} changes. It is because of this one observes only one peak in the composition variation of dielectric constant. In contrast, in BF-xBT, there is clear morphotropic phase transition from an average rhombohedral ($R3c$) structure to an average cubic ($Pm\bar{3}m$) and then from the average cubic to the tetragonal ($P4mm$) structure at $x \approx 0.35$ and 0.85, respectively.

D. Is the cubic structure truly cubic? Evidence for local disorder

BF-xBT samples sintered in oxygen atmosphere[26] or in the presence of dopants like Mn (Refs. 26,27) and Cu (Ref. 27) are insulating. In such samples, the so-called cubic compositions of BF-xBT are also reported to exhibit P-E hysteresis loop and Curie transition in ε'-T measurements characteristic of ferroelectricity.[26,27] As discussed in the introduction, the origin of ferroelectricity in the so-called cubic compositions is still under debate. However, our Rietveld refinements clearly reveal anomalously high values for the amplitude of thermal parameters of A and O sites for so-called cubic compositions close to $x = 0.35$ [see Fig. 5(d)]. The high amplitude of thermal parameters for A- and O-site ions is indicative of positional disorder, as reported in many Pb-based perovskites.[48–50] In order to capture the positional disorder in the average cubic phase of the BF-xBT system, we carried out high-energy, high-resolution synchrotron x-ray powder diffraction (SXRPD) measurements for cubic compositions with $0.40 \leqslant x \leqslant 0.85$. The synchrotron x-ray powder diffraction patterns shown in Fig. 8 do not exhibit any splitting or asymmetry in the 222_{pc}, 400_{pc}, and 440_{pc} pc profiles, in agreement with the rotating anode XRPD data shown in Fig. 1. However, when we carried out the Rietveld refinement of the structure of BF-0.40BT assuming ideal cubic $Pm\bar{3}m$ space group model, the fit between the observed and calculated profiles is satisfactory for lower 2θ regions only [see Fig. 9(a)]. On the higher 2θ regions [shown in the inset to Fig. 9(a)], the calculated intensities are lower than the observed intensities with large discrepancies for most of the reflections. The large discrepancy between the calculated and observed intensities in the higher 2θ region clearly suggests that the crystal structure of BF-0.40BT is not ideal cubic perovskite type, as suggested by low-energy rotating anode-based XRPD data. It is worth mentioning here that the use of high-energy SXRPD data enables the observation of peaks with significant intensities even at very high q values, at which the rotating anode data shows insignificant intensity above the background count.

One of the reasons for positional disorder at the Bi^{3+}/Ba^{2+} could be the large size difference between the ionic radii of the Bi^{3+} ($r = 1.17$ Å) and Ba^{2+} ($r = 1.36$ Å).[51] Because of smaller size of Bi^{3+}, it may occupy off-centered positions in the cubo-octahedral cage of oxygen ions. Such an off-centering would lead to departure from average cubic structure locally. To capture this, we first considered local off-center displacement of Bi^{3+} along the ⟨100⟩, ⟨110⟩, and ⟨111⟩ directions separately using split-site refinement for the average cubic structure.[38]

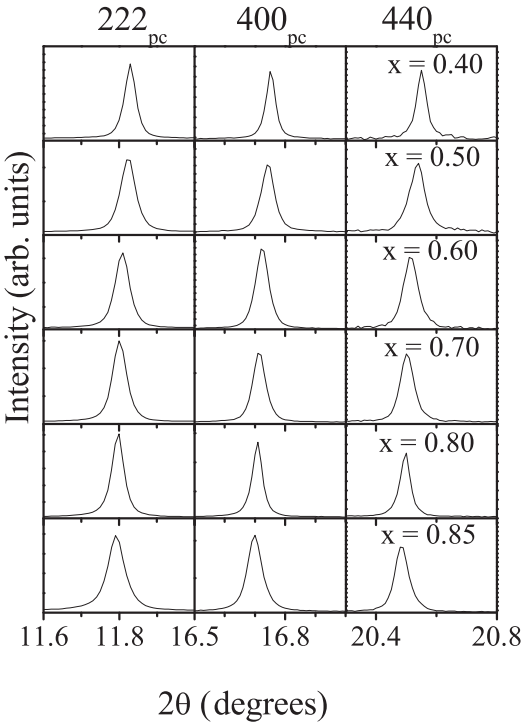

FIG. 8. Room temperature SXRPD profiles of the 222_{pc}, 400_{pc}, and 440_{pc} pc reflections of BF-xBT for $x = 0.40$, 0.50, 0.60, 0.70, 0.80, and 0.85.

Figure 10(a) shows the weighted profile agreement factor R_{wp} for various values of off-center displacements of Bi^{3+} along the symmetry directions in BF-0.40BT. It is evident from the figure that minimum in R_{wp} is the deepest for the displacements in the ⟨100⟩ direction revealing Bi^{3+} off-centering in the ⟨100⟩ cubic direction. The isotropic thermal parameter (B_{eq}) of Bi^{3+} decreases significantly with off-center displacement of Bi^{3+} along all the three ⟨100⟩, ⟨110⟩, and ⟨111⟩ directions, as shown in Fig. 10(b). We also considered the local displacement of Ba^{2+}, Fe^{3+}, and Ti^{4+} cations with respect to their special Wyckoff positions, but the R factors and the fitting features did not improve in the Rietveld refinements. However, for O^{2-}, we observe a well-defined minimum in the weighted profile agreement factor (R_{wp}) for displacement of oxygen along ⟨110⟩ (i.e., along the face diagonals of the cube) with respect to the (1/2, 1/2, 0) special position as shown in Fig. 10(c). The consideration of displacement of O^{2-} along the ⟨100⟩ and ⟨111⟩ directions does not reveal any minima, as can be seen from the same figure. The decrease in the isotropic thermal parameter of oxygen corresponding to displacement of O^{2-} along the three ⟨100⟩, ⟨110⟩, and ⟨111⟩ directions is shown in Fig. 10(d). In spite of the off-centering of Bi^{3+} along ⟨001⟩ by 0.48 Å, the anisotropic thermal parameters of Bi^{3+} along the [110] direction are still an order of magnitude larger than that in the [001] direction ($\beta_{11} = \beta_{22} = 0.05$, $\beta_{33} = 0.005$). More significantly, the equivalent isotropic thermal parameter $B_{eq} = 2.4$ Å^2 is still quite high. This indicates that, in addition to off-centering of Bi^{3+}along the ⟨001⟩ direction, there is the possibility of off-centering of Bi^{3+} along the x and y directions as well. We therefore considered the off-centered displacement of equal magnitude (to preserve the average cubic symmetry)

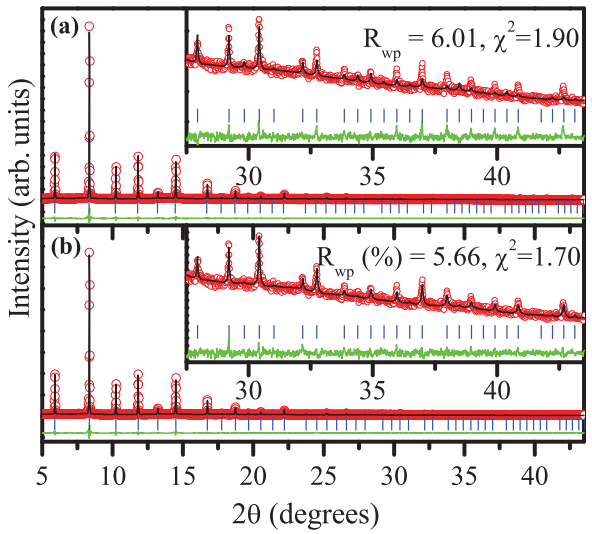

FIG. 9. (Color online) Observed (circles), calculated (line), and difference (bottom line) patterns obtained after the Rietveld analysis of SXRPD data of BF-0.40BT at room temperature using (a) average cubic structure and (b) disorder Bi^{3+} along the ⟨001⟩ and ⟨110⟩ directions and O^{2-} along the ⟨110⟩ direction in the average cubic structure with $Pm\bar{3}m$ space group. The vertical tick marks correspond to the positions of Bragg reflections. The insets in (a) and (b) depict the fits for high-angle reflections on a magnified scale.

along the x and y directions, i.e., the ⟨110⟩ direction also, in addition to Bi^{3+} and O^{2-} local displacements along the ⟨001⟩ and ⟨110⟩ directions, respectively, in the refinements. We find that there is only a marginal improvement in the fit with a decrease in R_{wp} by 1% (i.e., from 5.67 to 5.66) for off-centered displacement of Bi^{3+}($d \sim 0.23$ Å) along the ⟨110⟩ direction, but interestingly the amplitude of the thermal parameter of Bi^{3+} becomes isotropic and drops drastically to a reasonable value of 0.4 $Å^2$ from the unrealistically large value of 2.4 $Å^2$. We thus conclude that Bi^{3+} goes off-center from the cube corner positions like (0,0,0) to (x,x,z) positions while O^{2-} shifts from the center of the face (0.5,0.5,0) to

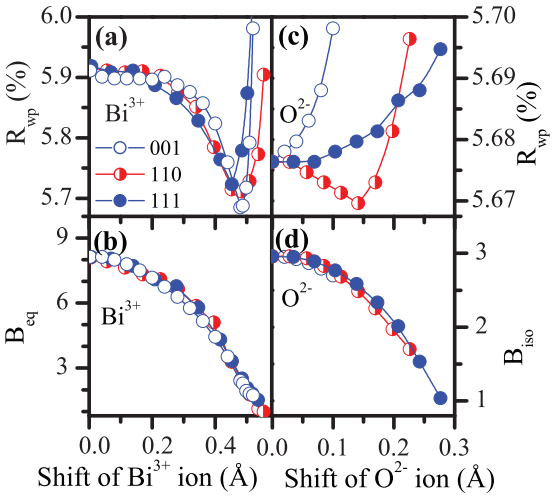

FIG. 10. (Color online) Variation of weighted profile agreement factors R_{wp}(%) and thermal parameters B_{iso}/B_{eq} with off-center displacement of (a) and (b) Bi^{3+} and (c) and (d) O^{2-} for BF-0.40BT.

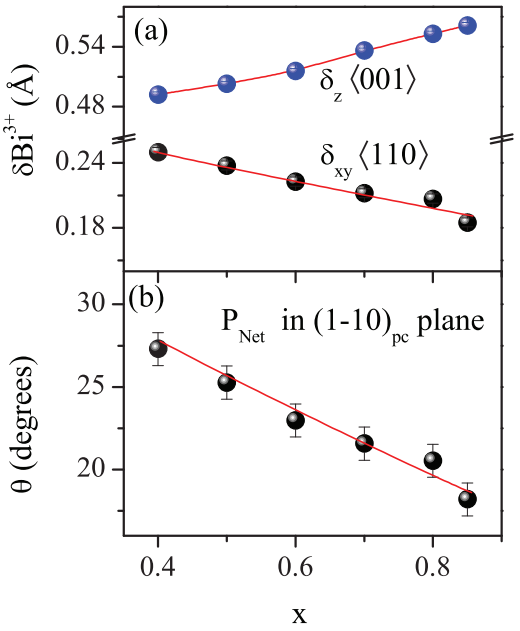

FIG. 11. (Color online) Variation of (a) off-center displacement of Bi^{3+} along the ⟨110⟩ and ⟨001⟩ directions and (b) polarization rotation angle with respect to the [001] direction on the $(1\text{-}10)_{pc}$ plane with x for various pc compositions of BF-xBT with $x = 0.40$, 0.50, 0.60, 0.70, 0.80, and 0.85.

(y,y,0) positions. The (x,x,z) and (y,y,0) positions correspond to general Wyckoff sites 24m and 12i.[52] So our refinements using high-energy x-ray powder diffraction data reveal the occupancy of some of the general positions in the average cubic structure. Figure 9(b) depicts the Rietveld fit for SXRPD data on BF-0.40BT using both Bi^{3+} and O^{2-} positions at (x,x,z) and (y,y,0), respectively. The fit between the observed and calculated profiles has improved significantly, as can be seen from a comparison of the inset to Fig. 9(b) with that in Fig. 9(a). In a similar way, we have also analyzed the SXRPD data for other compositions in the range $0.50 \leqslant x \leqslant 0.85$. The results of the Rietveld refinement are given in Table S2 in the Supplemental Material.[41] We find that the off-center displacement of Bi^{3+} along [001] (z direction in the present case) increase with decreasing Bi^{3+} content, while it decreases along ⟨110⟩ (x and y directions) with increasing x. This is shown in Fig. 11(a). The off-center displacement of O^{2-} along ⟨110⟩ is rather small (~0.12 Å) for BF-0.40BT as compared with that of Bi^{3+}, and it decreases with increasing x drastically. As a result, we could capture O^{2-} disorder for $x = 0.40$ and 0.50 only. However, the anisotropic thermal parameters of O^{2-} for $0.60 \leqslant x \leqslant 0.70$ indicate the possibility of small positional disorder along ⟨110⟩ in $x = 0.60$ and 0.70 also, as can be seen from the large value of $\beta_{11} = \beta_{22}$ as compared with β_{33} in Table S2 in the Supplemental Material.[42] For still higher x values ($x > 0.70$), the oxygen thermal parameters are isotropic.

E. Implications of local disorder of O^{2-} and Bi^{3+}

1. *Local oxygen octahedral tilt*

In the rhombohedral ($R3c$) structure of $BiFeO_3$, the long-range ferroelectric order arises from the polar displacements of ions along $[111]_{pc}$ and is accompanied with tilting of

oxygen octahedra about $[111]_{pc}$ as well. As a result of $BaTiO_3$ substitution to $BiFeO_3$, both the polar displacements and oxygen octahedral tilting angle decrease and vanish in the ideal cubic structure for $0.35 \leqslant x \leqslant 0.85$. However, the Rietveld analysis of high-energy SXRPD data for the cubic compositions reveals local displacements of O^{2-} along $\langle 110\rangle_{pc}$ directions from their special positions. The $\langle 110\rangle_{pc}$ displacements of O^{2-} are equivalent to the rotation of oxygen octahedra about $\langle 111\rangle_{pc}$ direction. Therefore, our results reveal that the rhombohedral phase of BF-xBT loses its long-range ordered octahedral tilt at the $R3c$ to $Pm\bar{3}m$ transition, but this tilt persists locally beyond the phase transition composition ($x \geqslant 0.35$) even in the so-called cubic phase. The decrease in the displacement of O^{2-} with increasing x suggests that the local tilt disorder also decreases with decreasing $BiFeO_3$ concentration as expected.

2. *Ferroelectric polarization due to local Bi^{3+} disorder*

In ABO_3 type perovskite compounds, the tilt of oxygen octahedra does not break the inversion symmetry, and no ferroelectricity can be observed due to tilting of oxygen octahedra. Therefore, the observation of a ferroelectric P-E hysteresis loop in the so-called cubic phase of BF-xBT is due to the off-center displacement of the Bi^{3+} ion. One can estimate the polarization due to off-center displacement (x,x,z) of Bi^{3+} in the average cubic structure using point charge approximation by the expression: $P = (1/V)\sum_i q_i r_i$, where V is the volume of the unit cell and q_i is the charge on the ith atom with position vector r_i in the unit cell from the centrosymmetric position. For BF-0.40BT, the calculated ionic polarization obtained from the local Bi^{3+} disordered positions turns out to be $P \sim 25\ \mu C/cm^2$. This value is of the same order as observed experimentally ($P_r \sim 30\ \mu C/cm^2$) for the cubic phase of BF-0.35BT.[23] A good agreement between the experimentally observed ferroelectric polarization and our calculated values suggests that our local disorder model can account for the presence of ferroelectric polarization in the average cubic compositions of BF-xBT.

3. *Tricritical nature of ferroelectric-to-paraelectric transition for the pc compositions*

The off-center component displacement u_z and u_{xx} of Bi^{3+} along the [001] and [110] directions, respectively, is responsible for the ferroelectric nature of the cubic phase of BF-xBT. This off-center displacement serves as a microscopic order parameter and is expected to show a critical behavior as a function of temperature. Figure 12(a) shows the variation of $\langle 001\rangle_{pc}$ and $\langle 110\rangle_{pc}$ displacements in BF-0.70BT as a function of temperature. The variation of u_z follows $(T\text{-}T_C)^{1/4}$ with $T_C \sim 450$ K in agreement with our earlier work in BF-0.85BT.[38] However, u_{xx} displacement does not show any critical behavior. The net u_{xxz} displacement also follows $(T\text{-}T_C)^{1/4}$ dependence with $T_C \sim 450$ K, the temperature at which one sees an anomaly in the a parameter [see Fig. 12(b)] also. All these suggest that the dipoles associated with Bi^{3+} off-centering show the critical freezing with an exponent $\beta = 1/4$. This tricriticality is essentially due to the u_z displacement of Bi^{3+} ions.

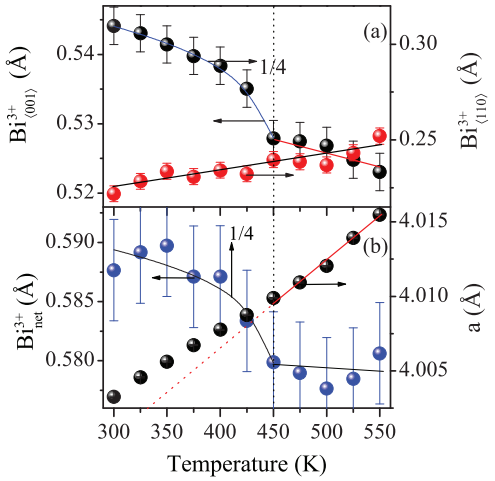

FIG. 12. (Color online) Variation of (a) off-center displacement of B^{3+} along the $\langle 001\rangle$ and $\langle 110\rangle$ directions and (b) the net displacement of Bi^{3+} along the [hhl] direction and the cubic unit cell parameter of BF-xBT for $x = 0.70$ as a function of temperature in the temperature range 300 to 550 K.

4. *Local monoclinic distortion of M_A-type and rotation of the polarization vector*

To understand the implication of local Bi^{3+} disorder in BF-xBT from the point of local symmetry breaking, a brief recapitulation of Vanderbilt and Cohen's theory using eighth-order expansion of the Landau free energy functional is required.[53] This theory predicts stability regions for three different types of monoclinic phases, namely M_A, M_B, and M_C, in addition to the tetragonal (T), rhombohedral (R), and orthorhombic (O) phases, which arise even in the sixth-order expansion of the free energy functional. Unlike the T, R, and O phases, where the polarization vector is confined to a specific crystallographic direction $\{\langle 001\rangle_{pc}$ for tetragonal [($P_X = P_Y = 0$, $P_Z \neq 0$), $\langle 011\rangle_{pc}$ for orthorhombic ($P_Y = P_Z$, $P_X = 0$), and $\langle 111\rangle_{pc}$ for rhombohedral ($P_X = P_Y = P_Z$)]$\}$, it lies on a plane of symmetry in the monoclinic phases. Here, the P_X, P_Y, and P_Z are the polarization component along the equivalent cube axes. In the monoclinic M_A ($P_X = P_Y < P_Z$) and M_B ($P_X = P_Y > P_Z$) phases, both in the Cm space group, the polarization vector rotates in the $\{1\text{-}10\}_{pc}$ plane. However, in the M_C ($P_X = 0$, $P_Y < P_Z \neq 0$) phase in the Pm space group, the polarization vector rotates on the $\{100\}_{pc}$ plane. The rotation of the polarization vector of the monoclinic phases on the symmetry plane does not affect the symmetry of the lattice. Because of this unique possibility of the rotation of the polarization vector in the monoclinic phases all the way from the $[001]_{pc}$ direction for the T phase towards the $[111]_{pc}$ direction of the R phase, the monoclinic phase(s) has (have) been termed as bridging phase(s) between the T and R structures.[43,54] In the PZT ceramics, the bridging phase is of M_A type in the Cm space group, as shown in Fig. 13(a).[43,54] In contrast, the PMN-xPT ceramics show the presence of M_B and M_C types in the Cm and Pm space groups, as shown in Fig. 13(b).[47] In principle, an orthorhombic phase should result on the point of crossing the M_B phase towards M_C, but such an orthorhombic phase has not been observed in

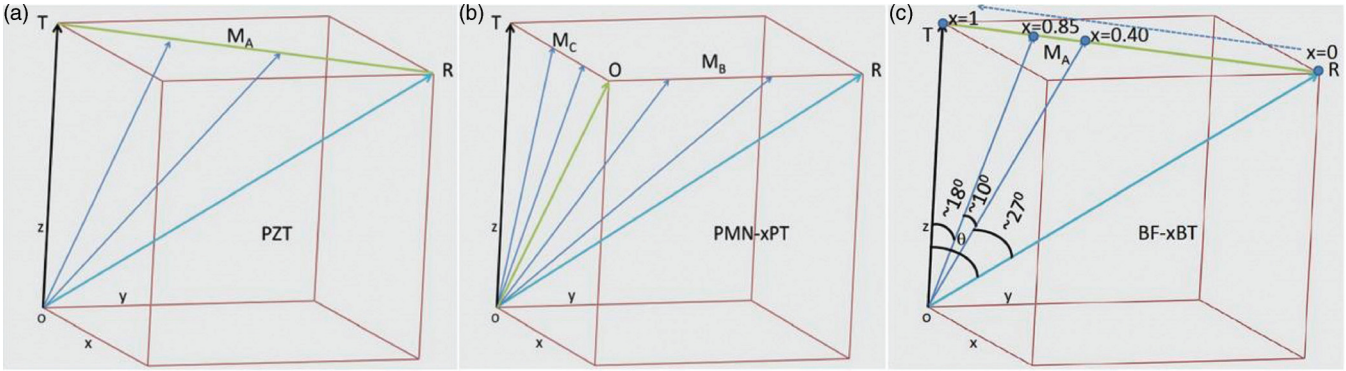

FIG. 13. (Color online) Schematic depiction of rotation of polarization vector from R to T phase in (a) PZT (R-M_A-T), (b) PMN-xPT (R-M_C-M_B-T), and (c) BF-xBT (R-M_A-T).

the PMN-xPT ceramics. Thus, the polarization rotation paths in the PZT and PMN-xPT are different. It is important to emphasize that, while crystallographic symmetry of the M_A, M_B, and M_C phases allows the rotation of polarization vectors on the $(1\text{-}10)_{pc}$, $(10\text{-}1)_{pc}$, and $(010)_{pc}$ planes, in reality this can occur only if the free energy surface on these planes is flat enough.[55,56]

In the cubic compositions of the BF-xBT system, the local Bi^{3+} displacements along the $[001]_{pc}$ and $[110]_{pc}$ directions imply development of polarization in a general $[hhl]$ direction on the (1-10) plane, as expected for the M_A-type monoclinic phase in the Cm space group. This reveals that the ferroelectric polarization in the "cubic" compositions of BF-xBT arises from the monoclinic distortions due to off-center displacements of Bi^{3+} along the $[hhl]$ direction with components along the $[001]_{pc}$ and $[110]_{pc}$ directions. The off-center displacement of Bi^{3+} along the $[hhl]$ direction arises due to the small ionic radius of Bi^{3+} as compared with Ba^{2+}, which disturbs the balance of the short-range electronic repulsion and long-range coulombic forces for the central position in the cubo-octahedral cage of O^{2-},[57] similar to what is well known in Sr-doped $CaTiO_3$ (Ref. 58) and Li-doped $KaTiO_3$.[59] The off-centering along $\langle 110\rangle_{pc}$ directions can also arise due to the hybridization of $6s^2$ lone pair orbitals of Bi^{3+} with $2p$ orbitals of O^{2-}.[60] It is probably because of this hybridization the component of the off-center displacements of Bi^{3+} along $[110]_{pc}$ decreases with decreasing $BiFeO_3$ concentration. We have calculated the angle of rotation (θ) of the polarization vector as a function of BT content (x) from the magnitude of local Bi^{3+} displacements given in Table S2 in the Supplemental Material.[42] The variation of this angle (θ) with x is shown in Fig. 11(b) and the corresponding polarization vectors in the Cohen's cube shown in Fig. 13(c) for various x values. It is evident from Fig. 11(b) that the polarization vector rotates continuously through 10° in a direction away from [111] of the rhombohedral towards [001] of tetragonal phases with increasing x. Such a large and continuous rotation of polarization vector has not been reported in other MPB systems like PZT and PMN-xPT either with respect to composition or with respect to the electric field.[61]

Before we close, a comparison of the monoclinic distorted pc phase of BF-xBT with the monoclinic and triclinic phases reported in the literature for epitaxially strained thin films of $BiFeO_3$ would be in order. In early studies, the structure of epitaxially strained thin films of $BiFeO_3$ was reported to be pseudotetragonal with a small monoclinic distortion as in the M_A phase of PZT in the Cm space group.[10] However, subsequent experiments revealed that the monoclinic phase may belong to the Cc space group as a result of the antiferrodistortive (AFD) rotation of oxygen octahedra[62,63] similar to the Cc phase reported in PZT ceramics.[43,64,65] More careful studies on the epitaxially strained films of $BiFeO_3$ have revealed a succession of phase transitions from the rhombohedral ($R3c$)-like structure of the bulk $BiFeO_3$ to the pseudorhombohedral M_A-type (Cc) monoclinic phase to the pseudotetragonal M_C type (Pm) monoclinic phase with increasing epitaxial strain.[66] This sequence has been confirmed by first-principles calculations also.[66] Since the transition from the M_A (Cc) to the M_C (Pm) phase cannot be continuous, an intermediate triclinic phase ($P1$) was predicted in these calculations and subsequently verified using synchrotron x-ray powder diffraction studies.[67] It is worth mentioning here that $PbTiO_3$ substitution in $BiFeO_3$ also leads to the stabilization of the M_A-type (Cc) monoclinic phase[68] with pseudorhombohedral features. The monoclinic phases reported in the $BiFeO_3$ thin films and $PbTiO_3$ substituted solid solutions show both polar and AFD long-range displacements of ions. In the case of BF-xBT, in marked contrast, we have found evidence for monoclinic distortion of M_A type in the pc compositions which do not show long-range polar and/or AFD displacements.

V. CONCLUSIONS

We have shown the appearance of two peaks in the composition dependence of the dielectric constant of BF-xBT at $x \approx 0.35$ and 0.85 due to a rhombohedral-to-cubic and a cubic-to-tetragonal morphotropic phase transition, respectively. We have shown that the true symmetry of the so-called cubic phase of BF-xBT, stable for $0.35 \leqslant x \leqslant 0.85$, is monoclinic of the M_A type in the Cm space group using high-energy SXRPD data. This monoclinic structure results from local displacement of Bi^{3+} leading to its occupancy at the xxz type general Wyckoff positions. The polarization vector of the monoclinic phase is shown to rotate in the $(1\text{-}10)_{pc}$ symmetry plane through 10°

on increasing the $BaTiO_3$ content from $x = 0.40$ to 0.85. The polarization results from local Bi^{3+} displacement and shows tricritical freezing as a function of temperature.

ACKNOWLEDGMENTS

D.P. and Y.K. acknowledge support from Department of Science and Technology (DST), Government of India and JSPS of Japan under the Indo-Japan Science Collaboration Program. A.S. acknowledges the award of extended Senior Research Fellowship of Council of Science and Industrial Research (CSIR), India and Project fellowship from University Grants Commission and Department of Atomic Energy (UGC-DAE), Consortium for Scientific Research, Indore, India. The synchrotron radiation experiments were performed at the BL02B2 of SPring-8 with the approval of the Japan Synchrotron Radiation Research Institute (Proposal Nos. 2011A1324 and 2011A0084).

*Corresponding author: dpandey_bhu@yahoo.co.in

[1] R. Ramesh and Nicola A. Spaldin, Nat. Mater. **6**, 21 (2007).
[2] W. Eerenstein, N. D. Mathur, and J. F. Scott, Nature (London) **442**, 759 (2006).
[3] M. Fiebig, J. Phys. D: Appl. Phys. **38**, R123 (2005).
[4] W. Kaczmarek and Z. Pajak, Solid State Commun. **17**, 807 (1975).
[5] Yu. E. Roginskaya, Tu. Ya. Tomashpolskii, Yu. N. Venevtsev, V. M. Petrov, and G. S. Zhdanov, Sov. Phys. JETP **23**, 47 (1966).
[6] I. Sosnowaska, T. Peterlin-Neumaier, and E. Steichele, J. Phys. C **15**, 4835 (1982).
[7] Yu. F. Popov, A. M. Kadomtseva, S. S. Krotov, D. V. Belov, G. P. Vorob'ev, P. N. Makhov, and A. K. Zvezdin, Low Temp. Phys. **27**, 478 (2001).
[8] Y. F. Popov, A. K. Zvezdin, G. P. Vorobev, A. M. Kadomtseva, V. A. Murashev, and D. N. Rokov, JETP Lett. **57**, 69 (1993).
[9] T.-J. Park, G. C. Papaefthymiou, Athur J. Viescas, A. R. Moodenbaugh, and S. S. Wong, Nano Lett. **7**, 766 (2007).
[10] J. Wang, J. Neaton, H. Zheng, V. Nagarajan, S. Ogale, B. Liu, D. Viehland, V. Vaithyanathan, D. Schlom, U. Waghamare, N. Spaldin, K. Rabe, M. Wutting, and R. Ramesh, Science **299**, 1719 (2003).
[11] B. Ruette, S. Zvyagin, A. P. Pyatakov, A. Bush, J. F. Li, V. I. Belotelov, A. K. Zvezdin, and D. Viehland, Phys. Rev. B **69**, 064114 (2004).
[12] I. Sosnowska, W. Schafer, W. Kockelmann, K. H. Andersen, and I.O. Troyanchuk, Appl. Phys. A **74**, 1040 (2002).
[13] I. Sosnowska, R. Przenioslo, P. Fescher, and V. A. Murasov, J. Magn. Magn. Mater. **160**, 384 (1996).
[14] Q. Q. Wang, Z. Wang, X. Q. Liu, and X. M. Chen, J. Am. Ceram. Soc. **95**, 670 (2012).
[15] A. Singh, V. Pandey, R. K. Kotnala, and D. Pandey, Phys. Rev. Lett. **101**, 247602 (2008).
[16] N. Itoh, T. Shimura, W. Sakamoto, and T. Yogo, J. Ceram. Soc. Jpn. **117**, 939 (2009).
[17] S. Bhattacharjee, A. Senyshyn, H. Fuess, and D. Pandey, Phys. Rev. B **87**, 054417 (2013).
[18] N. Wang, J. Cheng, A. Pyatakov, A. K. Zvezdin, J. F. Li, L. E. Cross, and D. Viehland, Phys. Rev. B **72**, 104434 (2005).
[19] M. M. Kumar, S. Srinath, G. S. Kumar, and S. V. Suryanarayana, J. Magn. Magn. Mater. **188**, 203 (1998).
[20] J. S. Kim, C. I. Cheon, C. H. Lee, and P. W. Jang, J. Appl. Phys. **96**, 468 (2004).
[21] S. Chandarak, M. Unruan, T. Sareein, A. Ngamjarurojana, S. Maensiri, P. Laoratanakul, S. Ananta, and R. Yimnirun, J. Magnetics **14**, 120 (2009).
[22] T. Ozaki, S. Kitagawa, S. Nishihara, Y. Hosokoshi, M. Suzuki, Y. Noguchi, M. Miyayama, and S. Mori, Ferroelectrics **385**, 6155 (2009).
[23] Y. Wei, X. Wang, J. Jia, and X. Wang, Ceramic International **38**, 3499 (2012).
[24] A. Singh, A. Senyshyn, H. Fuess, T. Chatterji, and D. Pandey, Phys. Rev. B **83**, 054406 (2011).
[25] B. Jaffe, W. R. Cook, and H. Jaffe, *Piezoelectric Ceramics*. (Academic Press, New York, 1971).
[26] S. O. Leontsev and R. E. Eitel, J. Amer. Ceram. Soc. **92**, 2957 (2009).
[27] H. Yang, C. Zhoub, X. Liu, Q. Zhoub, G. Chen, W. Li, and H. Wang, J. Eur. Ceram. Soc. **33**, 1177 (2013).
[28] C. J. Stringer, T. R. Shrout, C. A. Randall, and I. M. Reaney, J. Appl. Phys. **99**, 024106 (2006)
[29] C. A. Randall, R. E. Eitel, B. Jones, T. R. Shrout, and D. I. Woodward, J Appl Phys **95**, 3633 (2004).
[30] S. M. Choi, C. J. Stringer, T. R. Shrout, and C. A. Randal, J. Appl. Phys. **98**, 034108 (2005).
[31] A. Moure, M. Alguero, L. Pardo, E. Ringgaard, and A. F. Pedersen, J. Eur. Ceram. Soc. **27**, 237 (2007).
[32] C. Zhou, A. Feteira, Xu Shan, H. Yang, Q. Zhou, J. Cheng, W. Li, and H. Wang, Appl. Phys. Lett. **101**, 032901 (2012).
[33] B. Noheda, J. A. Gonzalo, L. E. Cross, R. Guo, S. E. Park, D. E. Cox, and G. Shirane, Phys. Rev. B **61**, 8687 (2000).
[34] I. H. Ismailzade, R. M. Ismailov, A. I. Alekperov, and F. M. Salaev, Phys Status Solidi **68**, K81 (1981).
[35] M. Kumar, A. Srinivas, and S. V. Suryanarayana, J. Appl. Phys. **87**, 855 (2000).
[36] R. Kiyanagi, T. Yamazaki,Y. Sakamoto, H. Kimura, Y. Noda, K. Ohyama1, S. Torii, M. Yonemura, J. Zhang, and T. Kamiyama, J. Phys. Soc. J. **81**, 024603 (2012).
[37] D. Pandey and A. Singh, Bull. Mater. Sci. **32**, 361 (2009).
[38] A. Singh, C. Moriyoshi, Y. Kuroiwa, and D. Pandey, Phys. Rev. B **85**, 064116 (2012).
[39] E. Nishibori, M. Takata, K. Kato, M. Sakta, Y. Kubota, S. Aoyagi, Y. Kuroiwa, M. Yamakata, and N. Ikeda, Nucl. Instrum. Methods Phys. Res., Sec. A **467–468**, 1045 (2001).
[40] J. Rodriguez-Carvajal Laboratory, FULLPROF 2010, Laboratoire Leon Brillouin, CEA-CNRS, France.
[41] H. D. Megaw, Acta Crystallogr. Sect. A **31**, 161 (1975).
[42] See Supplemental Material at http://link.aps.org/supplemental/10.1103/PhysRevB.88.024113 for the results of Rietveld analysis of XRPD and SXRPD data for various compositions of BF-xBT.
[43] D. Pandey, A. K. Singh, and S. Baik, Acta Crystallogr. Sect. A **64**, 192 (2008).

[44]A. K. Joncher, *Dielectric Relaxation in Solids* (Chelsea Dielectrics Press, London, 1983).
[45]R. P. S. M. Lobo, R. L. Moreira, D. Lebeugle, and D. Colson, Phys. Rev. B **76**, 172105 (2007).
[46]F. Jona and G. Shirane, *Ferroelectric Crystals* (Pergamon Press Inc., London 1962).
[47]A. K. Singh and D. Pandey, Phys. Rev. B **67**, 064102 (2003).
[48]J. M. Kiat, G. Baldinozzi, M. Dunlop, C. Malibert, B. Dkhil, C. Menoret, O. Masson, and M. T. F. Diaz, J. Phys.: Condens. Matter **12**, 8411 (2000).
[49]C. Malibert, B. Dkhil, J. M. Kiat, D. Durand, J. F. Berar, and A. S. Bire, J. Phys.: Condens. Matter **9**, 7485 (2000).
[50]Ragini, R. Ranjan, S. K. Mishra, and D. Pandey, J. Appl. Phys. **92**, 3266 (2002).
[51]R. D. Shannon and C. T. Prewttt, Acta Crystallogr. Sect. B **25**, 925 (1969).
[52]International Tables for Crystallography Volume A: Space-Group Symmetry (1983).
[53]D. Vanderbilt and M. H. Cohen, Phys. Rev. B **63**, 094108 (2001).
[54]B. Noheda and D. E. Cox, Phase Transitions **79**, 5 (2006).
[55]H. Fu and R. E. Cohen, Nature (London) **403**, 281 (2000).
[56]D. Damjanovic, IEEE Trans. Ultrason. Ferroelectr. Freq. Control **56**, 1574 (2009).
[57]B. E. Vugmeister and M. D. Glinchuk, Rev. Mod. Phys. **62**, 993 (1990).
[58]J. G. Bednorz and K. A. Muller, Phys. Rev. Lett. **52**, 2289 (1984).
[59]F. Borsa, U. T. Höchli, J. J. van der Klink, and D. Rytz, Phys. Rev. Lett. **45**, 1884 (1980).
[60]P. Ravindran, R. Vidya, A. Kjekshus, H. Fjellvag, and O. Eriksson, Phys. Rev. B **74**, 224412 (2006).
[61]R. Guo, L. E. Cross, S. E. Park, B. Noheda, D. E. Cox, and G. Shirane, Phys. Rev. Lett. **84**, 5423 (2000).
[62]R. J. Zeches, M. D. Rossell, J. X. Zhang, A. J. Hatt, Q. He, C.-H. Yang, A. Kumar, C. H. Wang, A. Melville, C. Adamo, G. Sheng, Y. H. Chu, J. F. Ihlefeld, R. Erni, C. Ederer, V. Gopalan, L. Q. Chen, D. G. Schlom, N. A. Spaldin, L. W. Martin, and R. Ramesh, Science **326**, 977 (2009).
[63]B. Dupe, I. C. Infante, G. Geneste, P. E. Janolin, M. Bibes, A. Barthelemy, S. Lisenkov, L. Bellaiche, S. Ravy, and B. Dkhil, Phys. Rev. B **81**, 144128 (2010).
[64]R. S. Solanki, A. K. Singh, S. K. Mishra, S. J. Kennedy, T. Suzuki, Y. Kuroiwa, C. Moriyoshi, and D. Pandey, Phys. Rev. B **84**, 144116 (2011).
[65]R. S. Solanki, S. K. Mishra, A. Senyshyn, S. Yoon, S. Baik, N. S. Shin, and D. Pandey, Appl. Phys. Lett. **102**, 052903 (2013).
[66]H. M. Christen, J. H. Nam, H. S. Kim, A. J. Hatt, and N. A. Spaldin, Phys. Rev. B **83**, 144107 (2011).
[67]Z. Chen, S. Prosandeev, Z. L. Luo, W. Ren, Y. Qi, C. W. Huang, L. You, C. Gao, I. A. Kornev, T. Wu, J. Wang, P. Yang, T. Sritharan, L. Bellaiche, and L. Chen, Phys. Rev. B **84**, 094116 (2011).
[68]S. Bhattacharjee and D. Pandey, J. App. Phys. **107**, 124112 (2010).